International Journal of Nanomedicine

Dovepress
Taylor & Francis Group

Open Access Full Text Article

ORIGINAL RESEARCH

CD71-Targeted and ROS-Responsive Micelles for Homoharringtonine Delivery to Enhance Therapeutic Efficiency Against FLT3-ITD Acute Myeloid Leukemia

Yuqian Tang[1], Jiaxin Li[2], Wu Ye[3], Yiwen Du[1], Ying Zhang[1], Yankun Yang[1], Yunxia Ye[2], Yuping Gong[1]

[1]Department of Hematology, West China Hospital, Sichuan University, Chengdu, 610041, People's Republic of China; [2]Key Laboratory of Drug-Targeting and Drug Delivery System of the Education Ministry and Sichuan Province, Sichuan Engineering Laboratory for Plant-Sourced Drug and Sichuan Research Center for Drug Precision Industrial Technology, West China School of Pharmacy, Sichuan University, Chengdu, 610041, People's Republic of China; [3]National-Local Joint Engineering Research Center of Biodiagnostics & Biotherapy, The Second Affiliated Hospital of Xi'an Jiaotong University, Xi'an, 710000, People's Republic of China

Correspondence: Yuping Gong, Department of Hematology, West China Hospital, Sichuan University, Chengdu, 610041, People's Republic of China, Tel +86 18980601257, Email gong2025@wchscu.edu.cn

Purpose: The FMS-like tyrosine kinase 3- internal tandem duplication (FLT3-ITD) subtype of acute myeloid leukemia (AML) is associated with poor clinical outcomes. Homoharringtonine (HHT), a natural protein inhibitor, has shown strong activity against FLT3-ITD AML. However, its clinical use is limited by rapid clearance and systemic toxicity. To address these limitations, a CD71-targeted, ROS-responsive micelle (TDTP/HHT) was developed for precise and efficient HHT delivery.

Methods: CD71 expression was assessed in AML patient samples and cell lines. TDTP/HHT was prepared by self-assembly using a D-peptide ligand (^{D}T7) for CD71 targeting and a ROS-cleavable linker for stimuli-responsive drug release. Cellular uptake, cytotoxicity and signaling pathway inhibition were evaluated in vitro across AML cell lines with distinct FLT3 statuses. The therapeutic efficacy of TDTP/HHT was further validated in a disseminated AML xenograft mouse model.

Results: Cytotoxicity analysis revealed that FLT3-ITD AML is intrinsically sensitive to HHT. Analysis of patient samples and cell lines revealed high CD71 expression and elevated ROS levels in AML, most predominantly in the FLT3-ITD subtype. The designed TDTP/HHT showed prolonged circulation time, ROS-responsive drug release, and stable targeting capacity. It did not compete with endogenous transferrin for binding sites but instead demonstrated transferrin-promoted cellular uptake. Both in vitro and in vivo studies confirmed that TDTP/HHT significantly inhibited the growth of FLT3-ITD AML cells. Mechanistically, TDTP/HHT suppressed multiple key downstream signaling proteins of FLT3-ITD. In addition, the system also remained active in CD71-high FLT3-WT AML cells, although higher HHT concentrations were required.

Conclusion: This study presents a novel targeted nanodrug that exploits the intrinsic HHT sensitivity of FLT3-ITD AML cells and their characteristic high CD71 expression and elevated ROS levels. Therefore, this platform is particularly suited for the treatment of FLT3-ITD AML while potentially applicable to other AML subtypes with high CD71 expression. By enabling specific intracellular accumulation of HHT and multitarget inhibition of FLT3 signaling pathways, this system achieves enhanced anti-AML efficacy both in vitro and in vivo, offering strong potential for future clinical translation.

Keywords: acute myeloid leukemia, FLT3-ITD, homoharringtonine, CD71, targeted drug delivery, ROS responsive

Introduction

Acute myeloid leukemia (AML) is the most common adult hematologic malignancy, characterized by high aggressiveness and lethality.[1,2] Internal tandem duplication of FMS-like tyrosine kinase 3 (FLT3-ITD) is a common and clinically significant mutation that drives persistent downstream signaling that promotes leukemic cell proliferation, survival, and blocked

https://doi.org/10.2147/IJN.S588865
Received: 29 December 2025
Accepted: 27 April 2026
Published: 27 May 2026

differentiation.[3–5] Clinically, FLT3-ITD-positive AML is characterized by elevated white blood cell counts, poor response to standard chemotherapy, and early relapse.[6,7] These highlight the urgent need for more effective therapies.

Homoharringtonine (HHT), a natural alkaloid derived from Cephalotaxus species, has attracted international interest in hematologic malignancies. Its semisynthetic derivative, Omacetaxine mepesuccinate, has been approved for the treatment of chronic myeloid leukemia (CML) after failure of tyrosine kinase inhibitors.[8,9] However, the clinical application of HHT in AML remains largely limited to China, where it has been used as a first-line therapy for decades.[10–12] In this study, we demonstrated that HHT not only deregulates FLT3 expression but also exhibits superior anti-leukemic activity compared to gilteritinib, a more potent and selective second-generation FLT3 inhibitor. These findings suggest that HHT may serve as a promising alternative therapeutic strategy for FLT3-ITD AML, especially in the context of resistance, limited tolerability, and high cost associated with current FLT3-targeted agents. However, its clinical application is limited by a short half-life and nonspecific biodistribution, both of which contribute to systemic toxicity.[13,14] As the median AML diagnosis age is 68 and over 60% of FLT3-ITD patients are older than 60,[15–17] poor tolerance to intensive chemotherapy further limits HHT use in the elderly. These challenges highlight the need for improved delivery strategies, with nanodrug platforms offering a promising solution.

Nano-drug delivery systems (NDDSs) offer several advantages, including prolonged circulation time, controlled drug release, and improved tumor selectivity, without the need for chemical modification of the parent drug.[18–21] However, in AML, the enhanced permeability and retention (EPR) effect is limited due to absent solid tumor vasculature, making active targeting essential.[22,23] In this context, CD71 (also known as transferrin receptor 1, TfR1), a type II transmembrane glycoprotein involved in iron uptake, emerges as a promising target.[24,25] CD71 is highly expressed on AML cells across various genetic backgrounds, while showing restricted expression on normal blood cells, offering a broad-spectrum and selective delivery target.[26,27] Currently, the ligands used in CD71-targeted NDDS for AML include transferrin (Tf), ferritin, and monoclonal antibodies.[27–30] However, the high plasma levels of endogenous Tf (200–300 mg/dL) may compete with tumor CD71 binding,[31–33] potentially limiting the targeting efficiency of CD71-directed delivery systems. To address this limitation, the ^{D}T7 peptide was incorporated as an alternative CD71-targeting ligand. It is a D-amino acid peptide that selectively binds CD71, avoiding competition with endogenous Tf, and resistance to proteolysis.[34–36] To our knowledge, the application of ^{D}T7 in AML has not yet been explored.

In this study, we leveraged the potent anti-leukemic activity of HHT against FLT3-ITD AML and addressed its clinical limitations by developing a nanocarrier that that enables targeted and controlled drug release. The platform incorporates ^{D}T7 to avoid competition with endogenous Tf. To further enhance intracellular delivery and efficacy, a reactive oxygen species (ROS)-responsive design was incorporated. Elevated ROS levels in AML cells provide an intrinsic trigger for drug release,[37–39] especially in FLT3-ITD AML. The FLT3-ITD mutation constitutively activates the STAT5 protein. Activated STAT5 can bind to and recruit RAC1, thereby promoting the assembly of NADPH oxidase and the generation of ROS.[40–42] Consequently, cells harboring the FLT3-ITD mutation exhibit elevated intracellular ROS levels. This integrated strategy (CD71-targeting drug delivery and ROS-responsive drug release) aims to reduce systemic toxicity and enhance the therapeutic index of HHT for FLT3-ITD AML (Figure 1).

Material and Methods

Materials

Reagents involved in this study are listed in Supplementary Table 1.

CD71 Expression Analysis

For patient samples, 1×10^6 cells were used per sample; for cell lines, 2×10^5 cells were used. Cells were divided into control and experimental groups. Control samples were stained with CD45-FITC, CD34-APC/Cy7 and isotype control antibodies, while experimental samples were stained with CD45-FITC, CD34-APC/Cy7 and CD71-APC. Staining was performed at room temperature for 15 min, washed, and analyzed by flow cytometry (Navios, Beckman Coulter, USA) to assess CD71 expression.

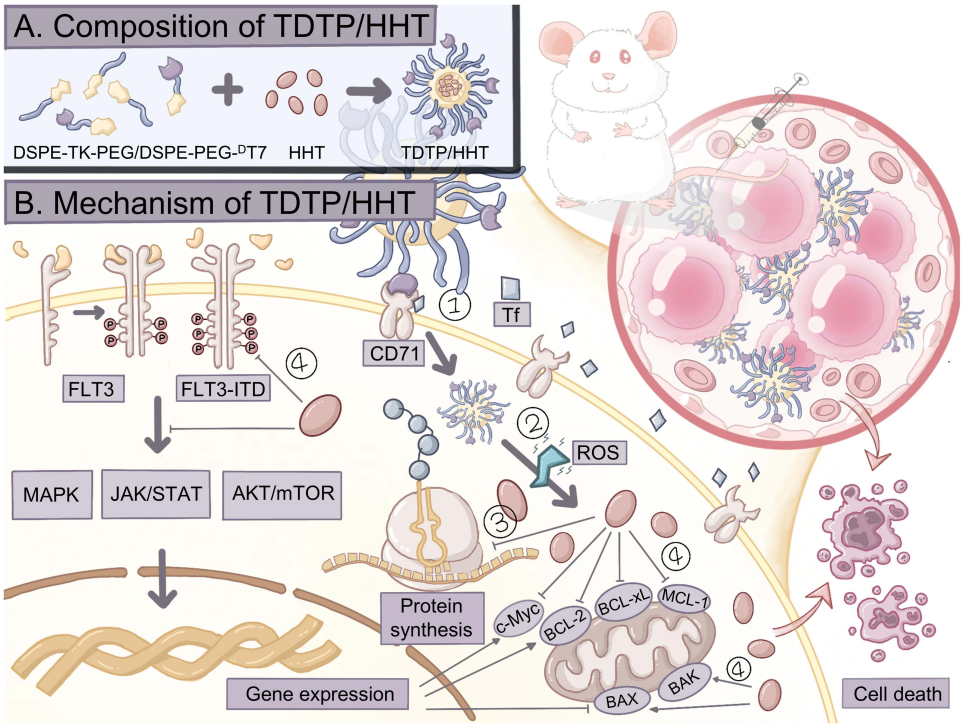

Figure 1 Schematic illustration of the TDTP/HHT nanoplatform. (**A**) Composition of the TDTP/HHT micelle; (**B**) Proposed mechanism of action: ① TDTP/HHT specifically binds to CD71 and is internalized via receptor-mediated endocytosis; ② Intracellular ROS trigger the release of encapsulated HHT; ③ Released HHT inhibits protein synthesis; ④ Downregulation of FLT3 expression and modulation of its downstream signaling pathways.

ROS Level Detection

Cells (5×10^5) in logarithmic growth phase were divided into control and experimental groups. Control samples received 100 μL FBS-free medium, while experimental samples were treated with 100 μL FBS-free medium containing 50 μg/mL DCFH-DA. Following a 30-minute incubation at 37 °C, cells were washed three times with FBS-free medium, centrifuged, resuspended in 300 μL PBS, and analyzed by flow cytometry to assess ROS levels.

For analysis of ROS level after HHT exposure, cells (1×10^5) in logarithmic growth phase were seeded into 6-well plates and treated with PBS or 20 nM HHT for 24 h. Then cells were collected and stained using the same protocol.

Preparation and Characterization of Micelles

HHT-loaded micelles (TDTP/HHT) were prepared via the emulsification-solvent evaporation method. Briefly, DSPE-TK-PEG_{2000}, DSPE-$mPEG_{2000}$-^{D}T7, and HHT (92:8:2.5, w/w) were dissolved in chloroform, stirred for 30 min, and mixed with PBS (7× chloroform volume). The mixture was ultrasonicated (100 W for 5 min with 5 s on / 5 s off), followed by chloroform removal via rotary evaporation (55 °C) and ultrafiltration to eliminate free HHT. Non-targeting micelles were prepared by replacing DSPE-$mPEG_{2000}$-^{D}T7 with DSPE-$mPEG_{2000}$.

For drug-loading analysis, micelles were disrupted in methanol (v/v=1:5), and HHT concentration was quantified by high-performance liquid chromatography (HPLC; Agilent 1200 Series, Palo Alto, USA) at 290 nm. Drug loading (%) was calculated as: (mass of encapsulated HHT / total HHT mass in micelles)×100. The zeta potential and hydrodynamic diameter were measured using a laser particle size analyzer (ZS90, Malvern Instruments Ltd., UK). Morphology was observed by transmission electron microscopy (TEM; JEM-1400FLASH, JEOL, Japan). Final micelles were sterilized with 0.22 μm filters for subsequent in vitro and in vivo experiments.

For uptake and biodistribution studies, fluorescent micelles were prepared by substituting HHT with DiD.

https://doi.org/10.2147/IJN.S588865

In vitro Drug Release

Micelles were dispersed in PBS or PBS containing 10 mM H_2O_2 at a final concentration of 1 mg/mL and incubated at 37 °C with gentle shaking. At designated time points (0.5, 1, 2, 4, 8, 12, and 24 h), samples were collected and subjected to ultrafiltration. The volume of the filtrate was recorded, and the concentration of HHT was quantified by HPLC. The cumulative release of HHT was then calculated accordingly. The release half-life ($t_{1/2}$) was calculated using linear interpolation according to the equation: $t_{1/2}=t_1+(50-R_1)/(R2-R_1)\times(t_2-t_1)$, where t_1 and t_2 represent the two time points before and after the cumulative release reaches 50%, and R_1 and R_2 denote the corresponding cumulative release percentages.

Uptake Assay

For patient samples, 5×10^5 cells were incubated with DiD-labeled micelles (final DiD 1.2 μg/mL). For cell lines, logarithmically growing cells were harvested, washed with PBS, resuspended in FBS-free medium. A total of 3×10^5 cells were seeded per well in 12-well plates and treated with DiD-labeled micelles (final DiD 1.2 μg/mL). To investigate the role of ^{D}T7 in uptake, cells were pre-incubated with 0.5 mM free ^{D}T7 for 1 h before adding TDTP/DiD. To evaluate the effect of endogenous Tf on uptake, 0.5 mL of AML patient-derived plasma was added with TDTP/DiD. After 4 h incubation at 37 °C, cells were collected, washed three times with PBS, resuspended and analyzed by flow cytometry for DiD-positive populations.

For confocal microscopy, 1×10^6 cells were seeded per well in 6-well and treated following the same protocol. After incubation, cells were fixed in 5% paraformaldehyde at room temperature for 15 min, washed with PBS, and mounted in antifade mounting medium. Coverslips were gently placed to avoid air bubbles and sealed. Slides were air-dried and imaged using a laser scanning confocal microscope (FV3000, Olympus, Japan).

In vivo Target Ability

Nine 5-week-old female BALB/c-Nude mice were purchased from GemPharmatech and acclimated for one week. MOLM-13 cells in logarithmic growth phase were collected, washed, and resuspended with FBS-free medium. A total of 5×10^6 cells were subcutaneously injected into the anterior region of the right thigh of each mouse. When the tumor volume reached 150 mm^3, mice were randomly divided into 3 groups by tumor size.

One hour prior to micelle injection, mice in the "TDTP/DiD pretreated with ^{D}T7" group received an intravenous injection of free ^{D}T7 peptide at a dose of 10 mg/kg. DiD-labeled micelles were then administrated via tail vein at a dose of 0.2 mg/kg. Fluorescence distribution and intensity were monitored using a in vivo imaging system (IVIS, IVIS Spectrum, PerkinElmer, USA) at predetermined time points. After 48 h, mice were euthanized under deep anesthesia, and major organs and tumors were collected for ex vivo fluorescence imaging. The maximal tumor volume permitted was 1500 mm^3, and this limit was not exceeded at the experimental endpoint.

MTT

Cells in logarithmic growth phase were seeded in 96-well plates at a density of 1×10^4 cells per 90 μL. Blank wells received 90 μL FBS-free medium and peripheral wells sterile 200 μL PBS to prevent evaporation. After overnight incubation, 10 μL of drug solutions at various concentrations were added. The blank and control groups received an equivalent volume of PBS. Plates were incubated for 24, 48, or 72 h depending on the experimental design. Then, 20 μL MTT solution (5 mg/mL) was added to each well and incubated for 4 h. Next, 100 μL of SDS-HCl solubilization solution was added, and plates were incubated overnight at 37°C. Absorbance at 570 nm was measured. Cell viability was calculated as: Cell viability (%) = $(OD_{sample} - OD_{blank})/ (OD_{control} - OD_{blank}) \times100$.

In vivo Anti-AML Efficacy

Luciferase-expressing MOLM-13 cells were generated by lentiviral transduction for in vivo bioluminescence imaging. Female NCG mice (5 weeks old) were purchased from GemPharmatech and housed for one week. Mice were intravenously injected via tail vein with 5×10^5 luciferase-labeled MOLM-13 cells. Tumor burden was assessed at 48 h post-injection using IVIS. Mice with comparable tumor bioluminescence intensities were randomly assigned to

four groups, and treatment was initiated at 72 h post-injection. Mice were administered 1.5 mg/kg of each formulation intravenously through the tail vein every other day.

Two independent cohorts of mice were used for histopathological and survival analyses, respectively. For histopathological analysis (n=4 per group), mice received six doses and were euthanized on day 15, and major organs were collected. For survival analysis (n=10 per group), mice received a total of 15 doses with tumor progression monitored twice weekly by IVIS, and overall survival recorded. Mice showing signs of disease (weight loss, lethargy, hunching, ruffled fur, or hind limb paralysis) were humanely euthanized under deep anesthesia according to the approved protocol. Imaging data were analyzed using coded samples to minimize potential bias.

In vivo Biocompatibility Evaluation

Twelve six-week-old female BALB/c mice were purchased from GemPharmatech and acclimated for one week prior to the experiment. The mice were then randomly divided into four groups (n=3 per group) and treated with PBS, free HHT, DTP/HHT, or TDTP/HHT at a dose of 1.5 mg/kg. The formulations were administered every other day for a total of 5 doses, with the first administration designated as day 0. Body weight was recorded every two days throughout the treatment period. Forty-eight hours after the final administration, peripheral blood was collected for complete blood count (CBC) analysis and assessment of liver and kidney function parameters. The mice were subsequently euthanized, and the heart, liver, spleen, lung, kidney, brain, and hindlimb bones were harvested for histopathological examination.

Statistical Analysis

Statistical analyses were performed using GraphPad Prism version 10.4. Data are presented as mean ± standard deviation (SD). Comparisons between two groups were conducted using unpaired Student's t-tests. For multiple group comparisons, one-way or two-way ANOVA followed by Tukey's post hoc test was performed. Kaplan-Meier survival curves were analyzed using the Log rank test. A p-value less than 0.05 was considered statistically significant: $p < 0.05$ (*), $p < 0.01$ (**), $p < 0.001$ (***), $p < 0.0001$(****).

Results

FLT3-ITD AML Cells are Intrinsically Sensitive to HHT Treatment

For assessment of the sensitivity to HHT, AML cell lines with distinct FLT3 backgrounds were examined: HEL (FLT3-null; negligible wild-type FLT3 expression), MOLM-13 (FLT3-ITD) and MV4-11 (FLT3-ITD), others are wild-type FLT3 (FLT3-WT). As shown in Figure 2A and B, three AML cell lines exhibited IC_{50} values below 20 nM, including the c-KIT-mutant Kasumi-1 (17.3 nM) and two FLT3-ITD cell lines MOLM-13 (13.0 nM) and MV4-11 (18.6 nM). Notably, both c-KIT and FLT3 belong to the class III receptor tyrosine kinase (RTK) family. After 48 h of 20 nM HHT treatment, apoptosis was induced in only 20%±1.3% of cells in the most sensitive cell line without RTK mutations (NB4), whereas over 80% of FLT3-ITD cells were nonviable (Figure 2C and D). These results indicate that AML cells harboring RTK mutations are particularly sensitive to HHT, including FLT3-ITD cells.

In addition, we further compared HHT with gilteritinib (GIL), a more potent and selective second-generation FLT3 inhibitor, in FLT3-ITD cell lines. The IC_{50} values of HHT and GIL in MOLM-13 were 16.7 nM and 62.4 nM, respectively. In MV4-11, they were 17.7 nM and 42.3 nM, respectively (Figure 2E). These findings indicate that HHT exhibits comparable or even superior cytotoxicity to GIL in FLT3-ITD AML. Subsequent WB analysis revealed that HHT treatment significantly reduced total and phosphorylated FLT3 (p-FLT3) levels in both cell lines (Figure 2F), indicating that its cytotoxic effect involves suppression of FLT3 expression and signaling.

AML Cells Show Elevated CD71 Expression and ROS Levels, Predominantly in the FLT3-ITD Subtype

Given potent activity of HHT against FLT3-ITD AML, we next aimed to overcome its short half-life and nonspecific distribution by developing a CD71-targeted, ROS-responsive micellar system. Therefore, CD71 expression and ROS levels in AML cells were assessed before nanocarrier construction.

https://doi.org/10.2147/IJN.S588865

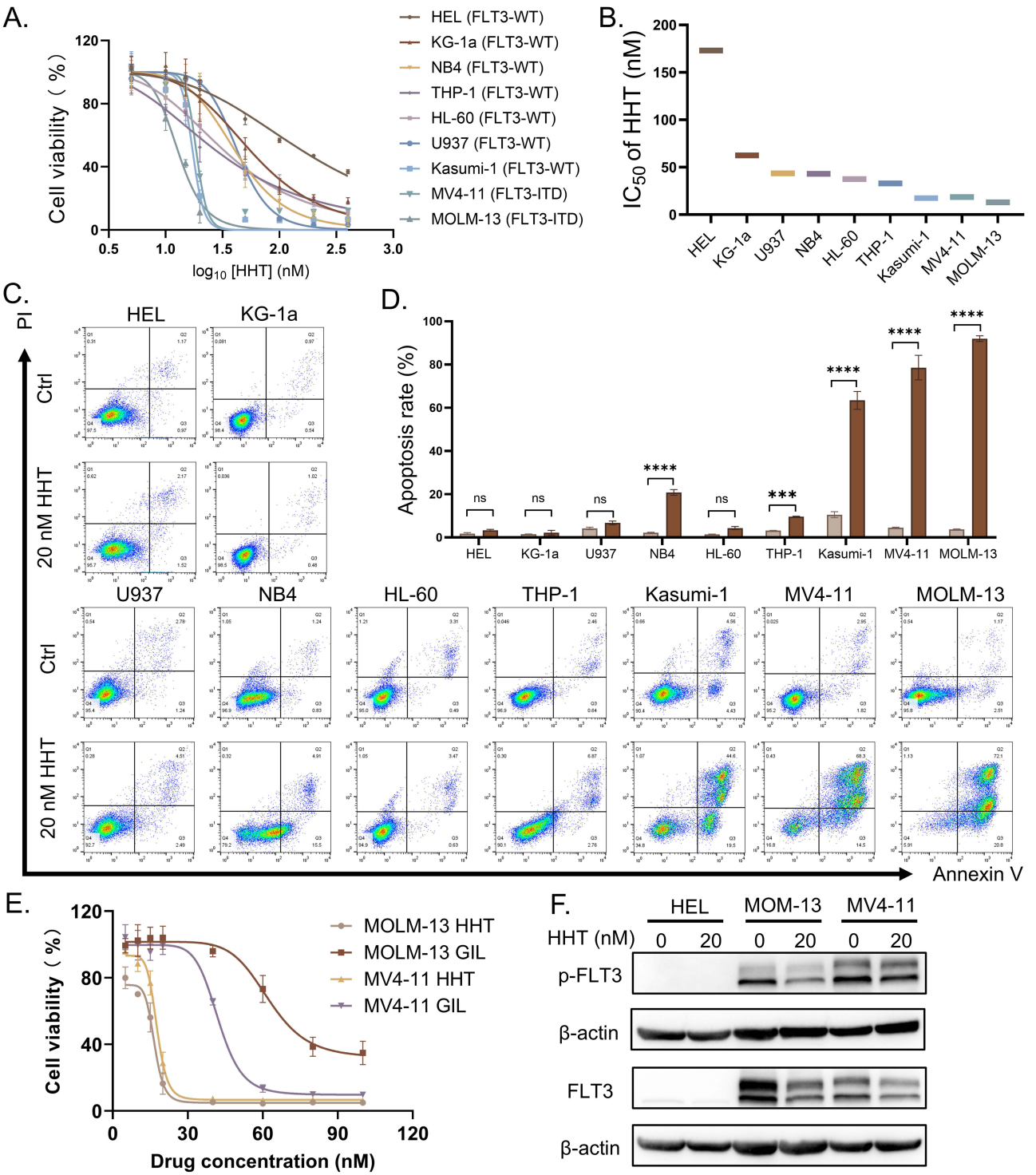

Figure 2 FLT3-ITD AML cells exhibit high sensitivity to HHT. (**A**) Dose-response curves of AML cell lines treated with HHT for 48 h (n=6). (**B**) IC_{50} of HHT in AML cell lines. (**C**) Apoptosis analysis of AML cell lines treated with HHT for 48 h. (**D**) Quantification of apoptotic cell populations shown in (**C**) (n=3). (**E**) MTT assay comparing the cytotoxicity of HHT and GIL in FLT3-ITD cell lines for 48 h (n=3). (**F**) WB analysis of total FLT3 and p-FLT3 levels in AML cells treated with HHT for 24 h. ***$p < 0.001$; ****$p < 0.0001$; ns, not significant.

Firstly, the CD71 expression in 55 bone marrow (BM) samples from primary AML patients was analyzed by flow cytometry. As shown in Figure 3A–C and Supplementary Figure 1A, CD71 was highly expressed on leukemia cells (LCs; median 80.1%, IQR=22.7%) and leukemia stem cells (LSCs; median 81.2%, IQR=19.8%), while showing limited

https://doi.org/10.2147/IJN.S588865

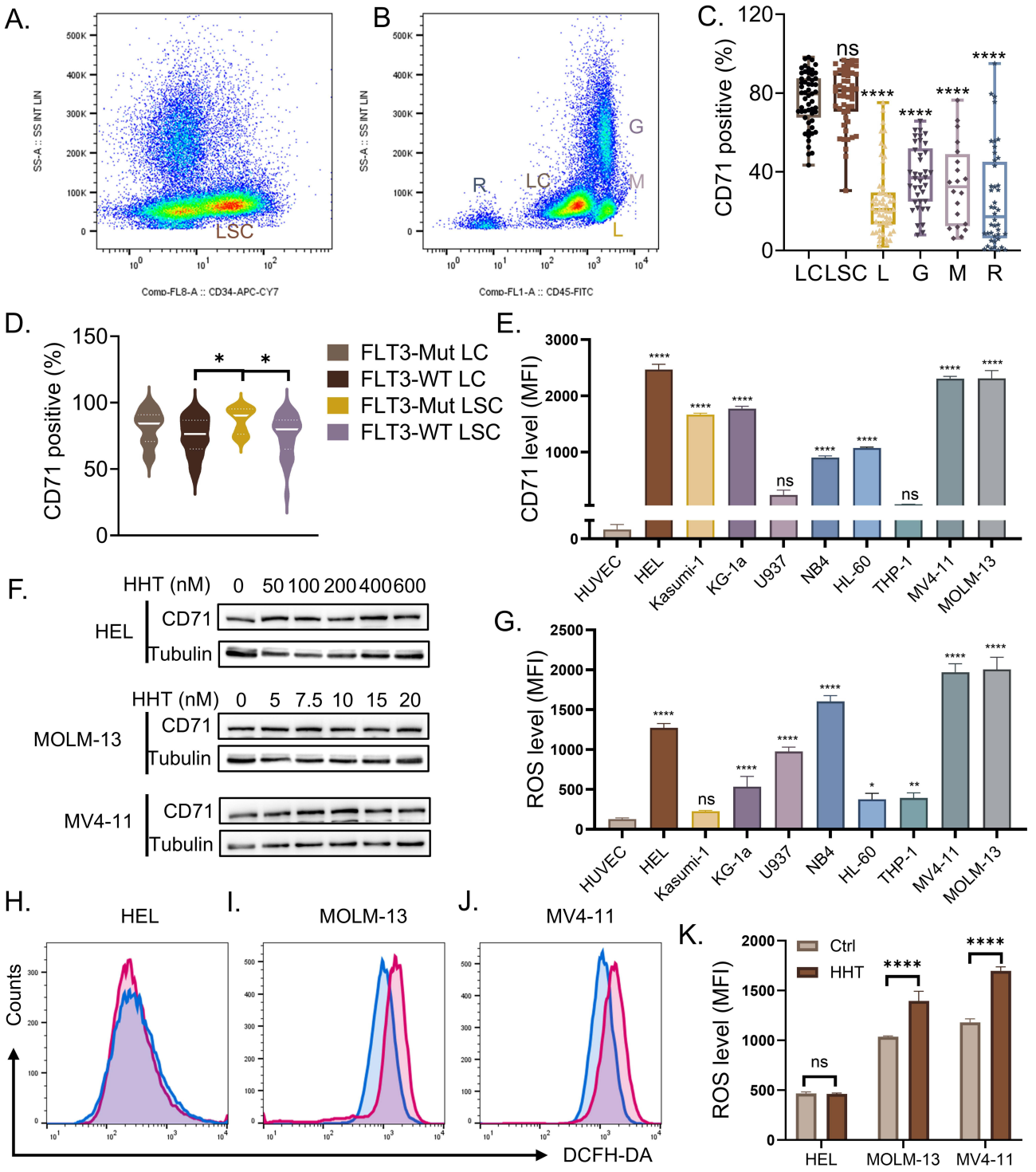

Figure 3 Elevated CD71 expression and ROS levels in AML cells, particularly in FLT3-ITD cells. (**A** and **B**) Flow cytometry plots of primary AML bone marrow samples showing gating strategy and subpopulations. (**C**) Quantified CD71 expression in leukemia cells (LCs), leukemia stem cells (LSCs), lymphocytes (L), granulocytes (G), monocytes (M), and nucleated red blood cells (R) (n=55). (**D**) Comparison of CD71 expression in LCs and LSCs between FLT3-mutated (n=15) and FLT3 wild-type (n=40) samples. (**E**) CD71 expression in AML cell lines compared to HUVECs (n=3). (**F**) WB analysis of CD71 expression after 24 h HHT exposure. (**G**) Intracellular ROS levels in AML cell lines and HUVEC (n=3). (**H–J**) Representative histograms of ROS levels after HHT treatment in HEL (**H**), MOLM-13 (**I**) AND MV4-11 (**J**). (**K**) Quantified ROS level in AML cells after HHT exposure (n=3). MFI, mean fluorescence intensity; Ctrl, control; *$p < 0.05$; **$p < 0.01$; ****$p < 0.0001$; ns, not significant.

expression on lymphocytes (L; median 20.8%, IQR=16.1%), granulocytes (G; median 37.8%, IQR=27.1%), monocytes (M; median 32.3%, IQR=36.6%), and nucleated red blood cells (R; median 20.6%, IQR=38.5%). Among these samples, 15 were FLT3-Mut and 40 were FLT3-WT. CD71 expression was higher in FLT3-Mut LCs (median 84.4%, IQR=20.1%)

https://doi.org/10.2147/IJN.S588865

compared to FLT3-WT LCs (median 80.2%, IQR=21.6%), and similarly elevated in FLT3-Mut LSCs (median 90.3%, IQR=19.0%) relative to FLT3-WT LSCs (median 79.9%, IQR=21.9%) (Figure 3D).

Consistent with patient samples, AML cell lines also exhibited high CD71 expression when compared to Human Umbilical Vein Endothelial Cells (HUVECs). Notably, FLT3-ITD cell lines showed higher levels than most other AML lines (Figure 3E). Therefore, HUVEC (low CD71) was selected as a normal control, and HEL, MOLM-13, and MV4-11 (high CD71) were used for subsequent experiments (Supplementary Figure 1B). Among them, HEL was used as a FLT3-null model, while MOLM-13 and MV4-11 were chosen as FLT3-Mut models. To determine whether HHT exposure would affect CD71 expression, AML cells were treated with various concentrations of HHT for 24 h and found CD71 expression remained unchanged (Figure 3F).

Due to a ROS-responsive mechanism was incorporated into the micelles to enable intracellular release, ROS levels were assessed using HUVEC as a normal control. ROS levels were significantly elevated in AML cell lines, with FLT3-ITD cells (MOLM-13 and MV4-11) showing the highest (Figure 3G). We further evaluated the effect of HHT treatment on intracellular ROS levels. As shown in Figure 3H–K, HHT exposure showed limited effect on FLT3-null cells, whereas it significantly increased ROS levels in FLT3-ITD cells.

Taken together, we found AML cells presented high CD71 expression with stable expression under HHT exposure, indicating that CD71 is a selective and reliable target for drug delivery. Moreover, AML cells showed elevated intracellular ROS levels, making ROS an ideal trigger for drug release. Importantly, both high CD71 expression and ROS levels are predominant in the FLT3-ITD subtype, highlighting the rationale for developing such a nanocarrier.

Preparation and Characterization of CD71-Targeted ROS-Responsive Micelles

To construct a CD71-targeted micellar carrier, the ^{D}T7 peptide (containing a terminal cysteine) was conjugated to DSPE-PEG_{2000}-Mal to generate DSPE-PEG_{2000}-^{D}T7. The successful synthesis was confirmed by ^{1}H-NMR and high-resolution mass spectrometry (HRMS) analysis (Supplementary Figure 2). Micelles were formulated using the emulsification-solvent evaporation method. To determine the optimal DSPE-PEG_{2000}-^{D}T7 modification ratio, DiD-labeled micelles containing varying percentages of DSPE-PEG_{2000}-^{D}T7 were incubated with AML cells. Fluorescence intensity analysis showed that uptake plateaued at an 8% modification level (w/w), which was therefore used for subsequent experiments (Supplementary Figure 3).

Dynamic light scattering (DLS) analysis revealed that the average diameters of DTP/HHT and TDTP/HHT were 115.7 ± 2.1 nm and 155.1 ± 14.6 nm, respectively, with low polydispersity (PDI= 0.15±0.04 and 0.13±0.02). TEM confirmed that both DTP/HHT and TDTP/HHT exhibited uniform spherical morphology (Figure 4A and B). The zeta potentials of DTP/HHT and TDTP/HHT were −3.7 ± 0.5 mV and −1.8 ± 0.5 mV, respectively, and their encapsulation efficiencies were 97.5% ± 1.9% and 96.7% ± 0.5% (Supplementary Figure 4). The critical micelle concentrations (CMC) were 3.0 μg/mL for DTP/HHT and 4.3 μg/mL for TDTP/HHT, indicating strong self-assembly stability.

For intravenous administration, hemolysis and plasma stability were evaluated. Both formulations showed negligible hemolysis and maintained high transmittance following plasma incubation, confirming favorable systemic safety (Figure 4C–E). In terms of functional responsiveness, the release half-life of TDTP/HHT in PBS was 3.4 h, whereas it decreased to 0.7 h in H_2O_2-containing media, representing an approximately 4.9-fold reduction. At the experimental endpoint (24 h), the cumulative release percentages were 61.5% in PBS and 93.4% in H_2O_2-containing media, respectively. These results indicate that TDTP/HHT exhibited accelerated HHT release in H_2O_2-containing media compared with PBS, confirming its ROS-triggered release behavior (Figure 4F). This responsiveness to oxidative conditions provides a mechanism for rapid intracellular release. To evaluate the effect of ^{D}T7 modification on circulation, DiD-labeled micelles were injected intravenously into BALB/c mice. In vivo imaging showed that fluorescence signals in the TDTP/DiD group were retained at higher levels over 72 h compared with the DTP/DiD group (Figure 4G). At the experimental endpoint, the whole-body fluorescence intensity in the DTP/DiD group decreased to approximately 76.9% ±2.1% of the initial level, whereas that in the TDTP/DiD group remained at approximately 85.2%±3.4%, suggesting that ^{D}T7 modification may prolong the circulation time of the micelles (Figure 4G and H).

Collectively, these results demonstrated the well-defined nanoscale structure, ROS-sensitive drug release, biocompatibility, and prolonged circulation time of the TDTP micellar system, which together support its potential for targeted and effective drug delivery in AML therapy.

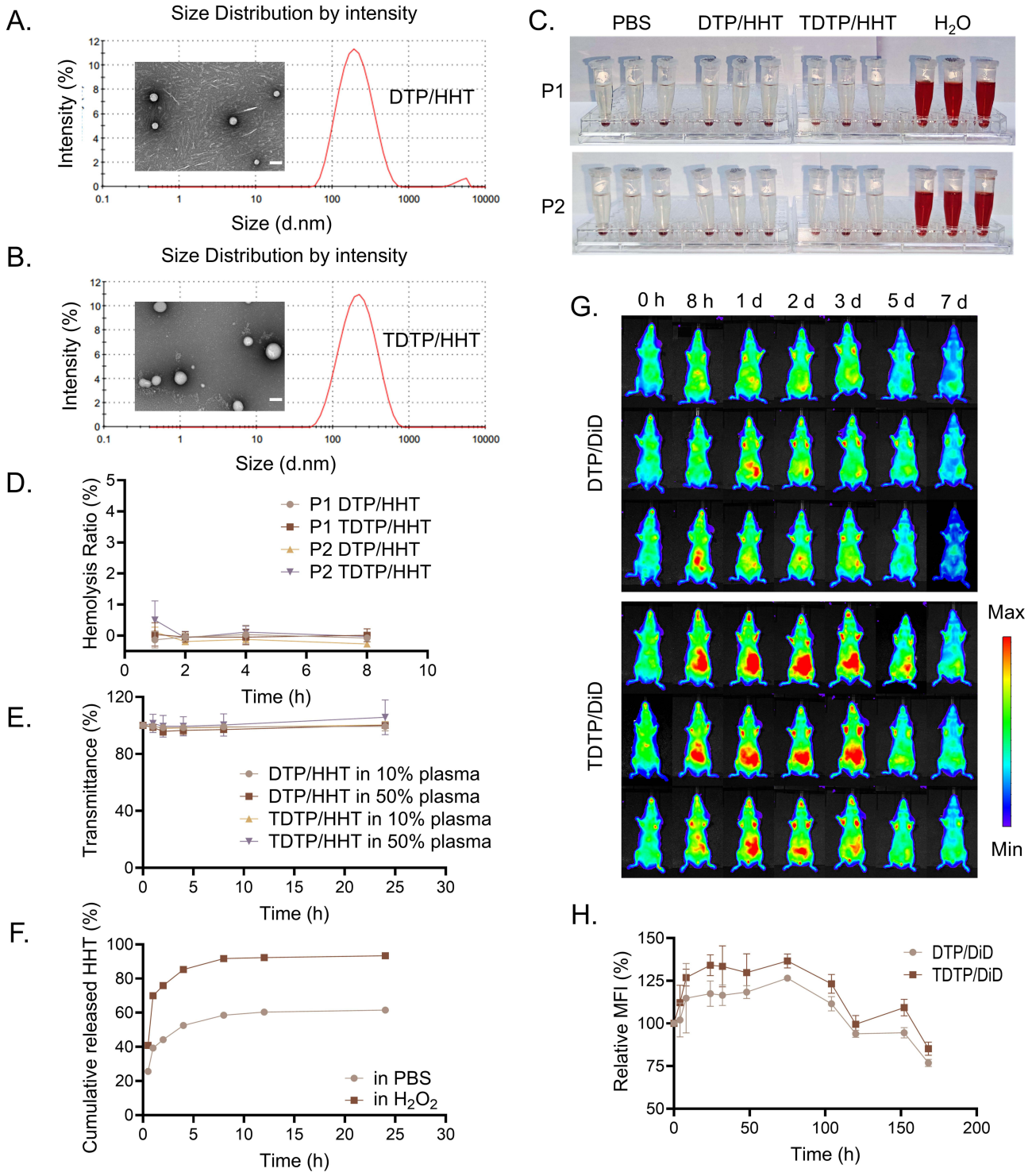

Figure 4 Characterization of HHT-loaded micelles. (**A** and **B**) TEM images and size distribution profiles of DTP/HHT (**A**) and TDTP/HHT (**B**), Scale bar=100 nm. (**C**) Representative images of hemolysis assay samples after 1 h incubation. (**D**) Quantitative hemolysis analysis of micelles incubated with AML patient peripheral blood (n=3). (**E**) Plasma stability of micelles over time (n=3). (**F**) Cumulative HHT release from TDTP/HHT in PBS or H_2O_2-containing media. (**G**) In vivo biodistribution of DiD-labeled micelles in BALB/c mice (n=3). (**H**) Relative fluorescence intensity of the mice shown in (**G**), normalized to the signal at 0 h (n=3). d, day.

The Micelles Display CD71-Dependent Cellular Uptake and in vivo Tumor Targeting

With the physicochemical profile of the micelles established, we proceeded to investigate the CD71-dependent targeting efficacy. Firstly, DiD-labeled formulations were incubated with AML patient-derived primary cells with high CD71

https://doi.org/10.2147/IJN.S588865

expression. TDTP/DiD showed markedly higher cellular uptake across all tested samples compared to DTP/DiD (Figure 5A), indicating improved targeting efficiency.

Subsequently, HUVECs (low CD71) and AML cell lines (MOLM-13, MV4-11, HEL; high CD71) were tested. In HUVECs, DTP/DiD exhibited the highest uptake (54.6% ± 8.3%), likely due to smaller particle size.[43,44] TDTP/DiD

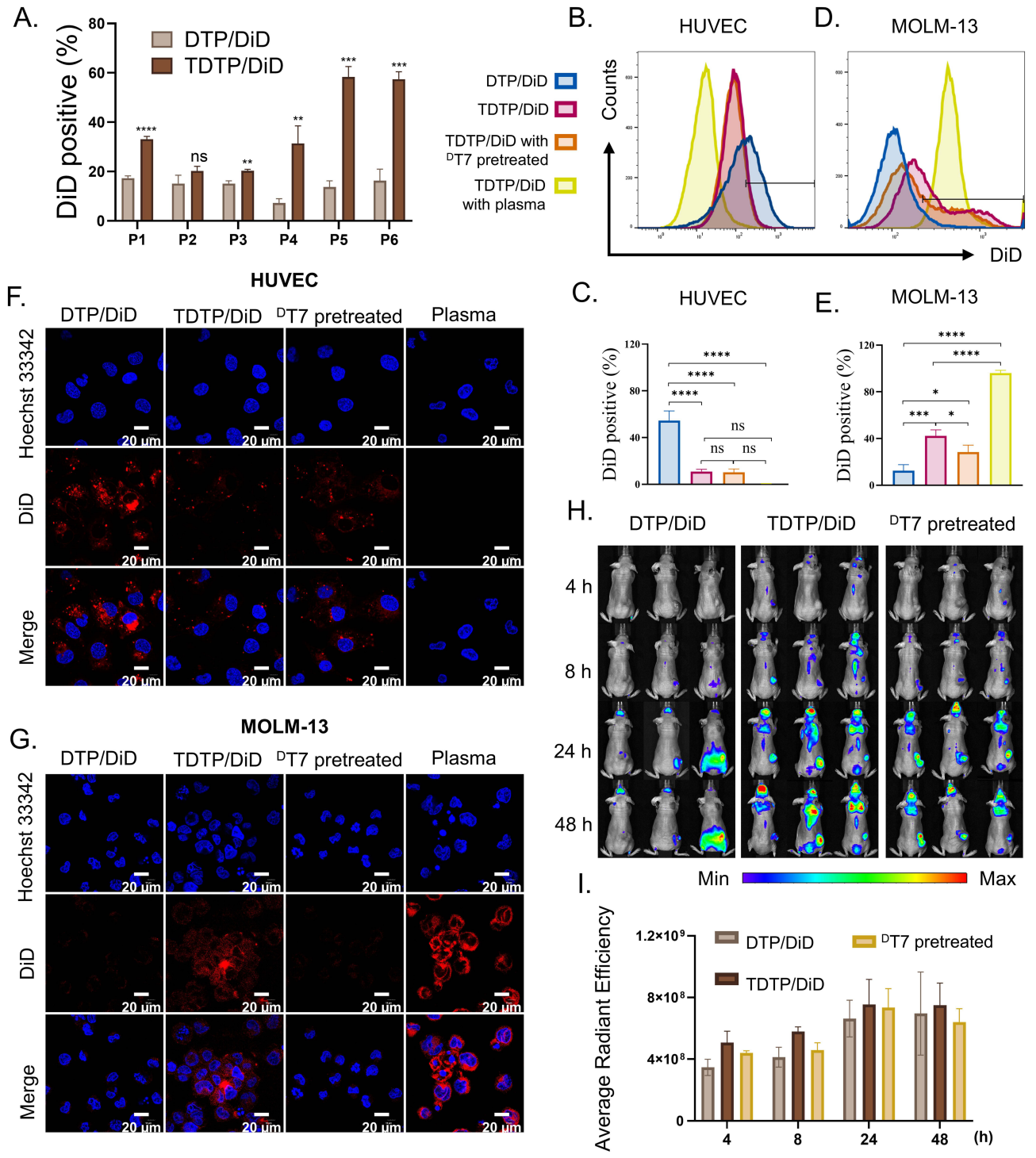

Figure 5 In vitro and in vivo evidence of CD71-mediated micelle uptake and tumor targeting. (**A**) DiD-positive cells of primary AML patient-derived cells following incubation with DTP/DiD or TDTP/DiD (n=3). (**B** and **C**) Representative flow cytometry histograms of HUVEC (**B**) and corresponding quantification of DiD-positive rates (**C**) (n=3). (**D** and **E**) Representative flow cytometry histograms of MOLM-13 (**D**) and corresponding quantification of DiD-positive rates (**E**) (n=3). (**F** and **G**) Confocal microscopy images of HUVEC (**F**) and MOLM-13 (**G**) treated with DiD-labeled micelles. Scale bar=20 μm. (**H**) IVIS images of AML xenograft mice following injection of DiD-labeled micelles (n=3). (**I**) Quantitative analysis of average radiant efficiency at tumor sites over time (n=3). *p < 0.05; **p < 0.01; ***p < 0.001; ****p < 0.0001; ns, not significant.

https://doi.org/10.2147/IJN.S588865

(10.9% ± 1.9%) and the free ^{D}T7 competition group (10.2% ± 2.8%) showed comparably low uptake, indicating ^{D}T7-independent internalization (Figure 5B and C). Notably, plasma incubation reduced uptake to 0.6% ± 0.1%. Microscopy revealed that EDTA-induced detachment of HUVECs into suspension decreased surface area, limiting micelle binding (Supplementary Figure 5). In contrast, MOLM-13 cells exhibited significantly higher uptake of TDTP/DiD (42.3% ± 5.2%) compared to DTP/DiD (12.4% ± 5.2%), and significantly reduced to 28.4% ± 5.9% upon free ^{D}T7 pre-treatment. These results confirm that TDTP micelle internalization is CD71-dependent. Plasma co-incubation further increased uptake to 96.0% ± 2.5%, suggesting that endogenous Tf does not compete with ^{D}T7 and even enhance uptake (Figure 5D and E). These results were further supported by confocal imaging (Figure 5F and G). Similar trends were also observed in another two CD71-high MV4-11and HEL cells (Supplementary Figure 6).

In vivo targeting was further evaluated in a subcutaneous AML xenograft model, where MOLM-13-bearing mice received intravenous DiD-labeled micelles. TDTP/DiD preferentially accumulated in tumors, exhibiting higher fluorescence than DTP/DiD (Figure 5H). At 8 h, the average radiant efficiency was higher for TDTP/DiD ($(5.80 \pm 0.30) \times 10^8$) than DTP/DiD ($(4.13 \pm 0.64) \times 10^8$), and decreased to $(4.58 \pm 0.47) \times 10^8$ by ^{D}T7 pre-treatment, further confirming CD71-mediated targeting (Figure 5H and I). At 48 h, ex vivo imaging revealed stronger fluorescence in tumors and organs from the TDTP/DiD-treated groups, consistent with prior in vivo imaging and pharmacokinetic data indicating prolonged circulation (Supplementary Figure 7).

Collectively, these results confirm that ^{D}T7-functionalized micelles retain CD71-mediated targeting capacity in both in vitro and in vivo settings.

TDTP/HHT Demonstrates Superior Anti-AML Activity in vitro Through Increased Cytotoxicity and Pathway Suppression

After validating targeting capability of ^{D}T7-modified micelles, we next evaluated their anti-AML efficacy in vitro. MTT assays were performed in FLT3-ITD AML cell lines with high CD71 expression. At 48 h, TDTP/HHT reduced the IC_{50} values from 11.8 nM to 7.5 nM in MOLM-13 (a 36.4% reduction), and from 18.0 nM to 9.8 nM in MV4-11 (a 45.6% reduction) (Figure 6A and B). Notably, DTP/HHT showed only modest improvements over free HHT. Similar trends were observed at 24 and 72 h (Supplementary Figure 8), with detailed IC_{50} values summarized in Supplementary Tables 2 and 3. Consistent with these findings, TDTP/HHT also showed the greatest cytotoxic effect in primary AML patient samples, indicating its clinical translational potential (Supplementary Figure 9 and Supplementary Table 4).

To further investigate the anti-leukemia effects of TDTP/HHT, soft agar colony formation and apoptosis assays were conducted. At equivalent doses, TDTP/HHT significantly reduced colony numbers by 37.6% in MOLM-13 (7.5 nM), and 87.3% in MV4-11 (10 nM) compared to the control group, outperforming both free HHT and DTP/HHT (Figure 6C–E). Consistently, TDTP/HHT induced highest apoptosis rates than controls. When treated for 48 h, TDTP/HHT triggered apoptosis in 61.5% of MOLM-13 and 36.5% of MV4-11 cells at 10 nM HHT, compared to 23.2% and 16.2% in free HHT groups, respectively (Figure 6F–H). We also evaluated the less sensitive FLT3-null and CD71-high cell line (HEL), TDTP/HHT still induced the most pronounced cytotoxicity while required a much higher dose (Supplementary Figure 10 and Supplementary Table 5). Together, these results suggest that ^{D}T7-mediated CD71 targeting significantly improves intracellular drug delivery and cytotoxicity, particularly in FLT3-ITD AML where elevated ROS levels may further facilitate drug release.

FLT3-ITD drives persistent downstream MAPK, PI3K/AKT/mTOR, and JAK/STAT signaling cascades, which promotes leukemic cell proliferation, survival, and blocked differentiation.[45–47] To elucidate the molecular basis of the enhanced cytotoxicity, WB analysis was performed to evaluate the inhibition of FLT3 and its downstream pathways. TDTP/HHT consistently induced the most reduction in both total and phosphorylated key signaling proteins across all tested pathways, compared to other groups at the same HHT concentration (Figure 6I and J). Consistently, oncogenic effectors (c-Myc, MCL-1, BCL-2, BCL-xL) were significantly downregulated, while pro-apoptotic proteins (BAX, BAK) were upregulated. These changes were also evident in FLT3-null HEL cells but need 40-fold higher HHT concentrations (Supplementary Figure 11), while FLT3-ITD cells only treated with 10 nM HHT, further conforming the advantage of targeted delivery in enhanced therapeutic effects in FLT3-ITD AML subtypes.

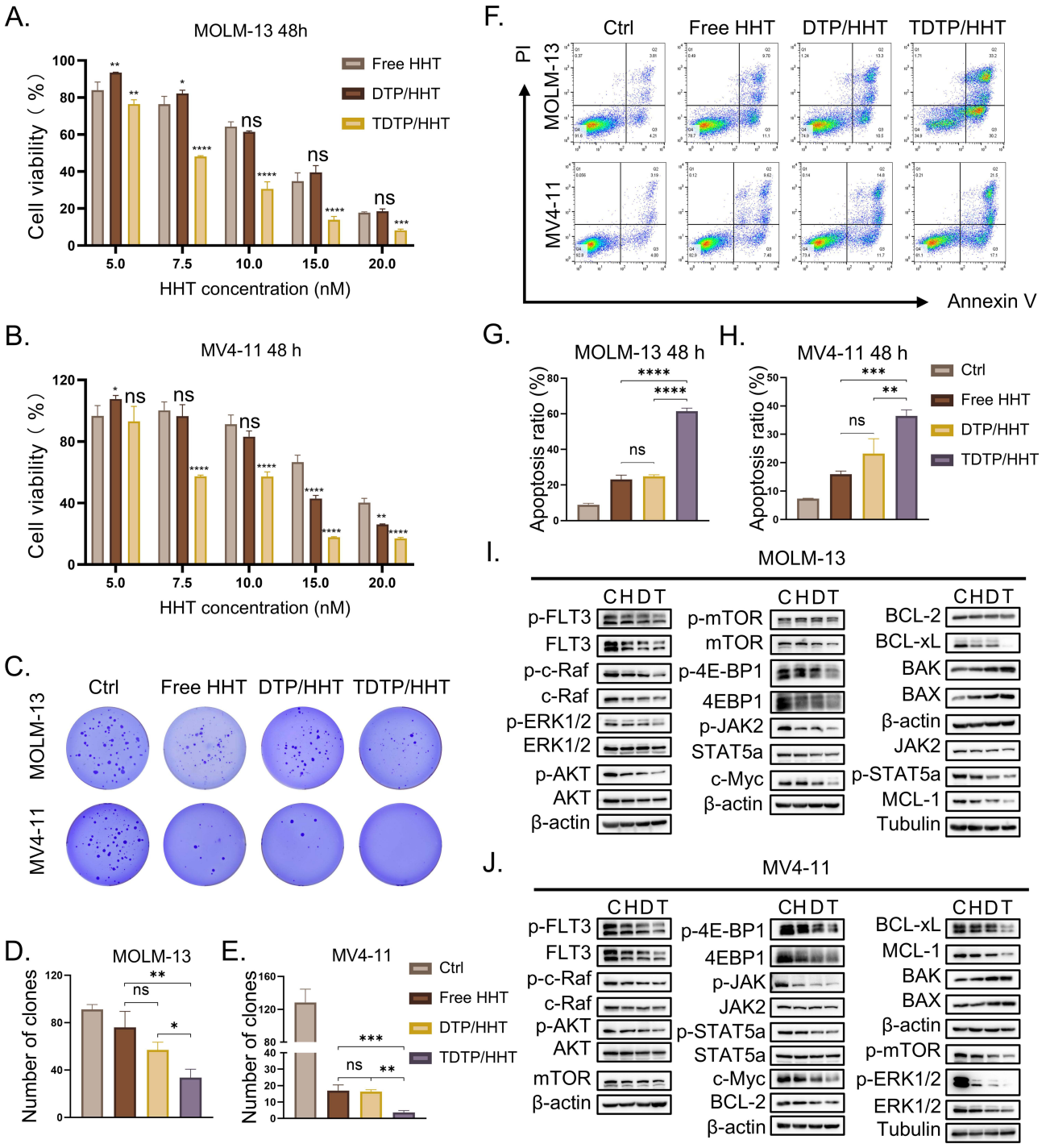

Figure 6 TDTP/HHT enhanced anti-AML efficacy through improved cytotoxicity and pathway inhibition. (**A** and **B**) MTT assays of different HHT formulations in MOLM-13 (**A**) and MV4-11 (**B**) after 48 h of treatment (n=3). (**C**) Representative images of soft agar colony formation in MOLM-13 (7.5 nM) and MV4-11 (10 nM) following treatment with different HHT formulations. (**D** and **E**) Quantification of colony numbers from (**C**) (n=3). (**F**) Apoptosis analysis in AML cell lines treated with different HHT formulations for 48 h (MOLM-13 and MV4-11: 10 nM). (**G**–**H**) Quantitative analysis of apoptosis data shown in (**F**) (n=3). (**I** and **J**) WB analysis of FLT3 signaling and downstream effectors treated with different HHT formulations in MOLM-13 (**I**) and MV4-11 (**J**). Ctrl/C, control; H, free HHT; D, DTP/HHT; T, TDTP/HHT; *$p < 0.05$; **$p < 0.01$; ***$p < 0.001$; ****$p < 0.0001$; ns, not significant.

Overall, these findings demonstrate that ^{D}T7-modified micelles enhance HHT efficacy in FLT3-ITD AML by promoting targeted delivery, increasing intracellular accumulation, and suppressing multiple key oncogenic signaling pathways.

https://doi.org/10.2147/IJN.S588865

TDTP/HHT Prolongs Survival and Reduces Tumor Burden in AML Mice

To evaluate the in vivo therapeutic efficacy of TDTP/HHT, a disseminated AML mouse model was established using luciferase-labeled MOLM-13 cells. On day 15 post-treatment, mice were euthanized and cells from BM, liver, and spleen were harvested and stained with human CD45-FITC antibody to quantify tumor burden by flow cytometry. The percentage of $CD45^+$ cells was significantly reduced in the TDTP/HHT group compared with free HHT and DTP/HHT (Figure 7A–D). Typically, $CD45^+$ populations in BM decreased from 74.0%±3.2% in the control group to 4.7% ±3.8% in the TDTP/HHT group (Figure 7B).

Histopathological evaluation further confirmed these findings. Representative sections of major organs (lower limb bone, liver, spleen and lung) were stained with hematoxylin and eosin (H&E) to assess leukemic infiltration. Mice treated with TDTP/HHT exhibited markedly lower infiltration in the BM, liver and lung compared to other groups (Figure 7E). Importantly, no signs of systemic toxicity, such as necrosis, inflammation, or tissue disorganization, were observed in any group (Supplementary Figure 12A). And treatment with TDTP/HHT resulted in the least body weight loss (Supplementary Figure 12B). These indicate good tolerability of the micellar formulations.

IVIS imaging revealed rapid disease progression of untreated MOLM-13 xenograft model (Figure 7F and G). HHT significantly reduced tumor burden (Figure 7H and I), DTP/HHT further delayed disease progression (Figure 7J and K), and TDTP/HHT achieved the most evident suppression (Figure 7L and M). All HHT formulations prolonged survival compared to controls (median survival: 19.5 days), extending to 28 days with HHT and 31 days with DTP/HHT. Notably, TDTP/HHT treatment further extended to 37 days, a 90% increase relative to controls and a significant improvement over both free HHT and DTP/HHT groups (Figure 7N). The superior survival benefit of TDTP/HHT demonstrated enhanced therapeutic efficacy conferred by dual-functional micellar delivery.

Different HHT Formulations Show Favorable in vivo Biocompatibility

Due to the propensity of AML cells to infiltrate organs such as the liver, spleen, and bone marrow, we further evaluated the in vivo biocompatibility of the micellar formulations in healthy BALB/c mice. Mice were administered PBS or different formulations of HHT. At the experimental endpoint, complete blood counts (CBC), along with liver and kidney function parameters, were analyzed, and major organs were collected for histopathological examination.

Body weight was monitored throughout the treatment period (Figure 8A). No significant differences in body weight changes were observed among all groups, suggesting that the treatments did not cause obvious systemic toxicity.

Given that CD71 is also expressed on early erythroid cells, CBC analysis was then performed (Figure 8B–D). The results showed that the levels of white blood cells (WBC), hemoglobin (Hb), and platelets (PLT) in mice treated with different HHT formulations were comparable to those in the PBS group, indicating that repeated administration of the various HHT formulations did not impair hematopoietic function. Although TDTP/HHT may accumulate in early erythroid cells, no anemia was observed in the treated mice.

Liver function was evaluated using alanine aminotransferase (ALT) and aspartate aminotransferase (AST), and no significant differences were observed among all groups (Figure 8E and F). Kidney function was assessed by measuring serum creatinine (CREA-S) and blood urea levels, which also showed no significant differences across all groups (Figure 8G and H). These results indicate that neither HHT nor the micellar carrier materials induced detectable hepatic or renal dysfunction.

Histopathological examination of major organs (heart, liver, spleen, lung, kidney, and bone marrow) after treatment revealed no apparent abnormalities (Figure 8I). The tissue architecture of all examined organs remained intact, with no evidence of inflammatory infiltration, necrosis, or structural damage. During the in vivo targeting assessment, fluorescence accumulation was also observed in the brain, similar to that detected at tumor sites. Therefore, brain sections were further evaluated by H&E staining. No neuronal loss, nuclear pyknosis, or neuronophagia was observed in any group (Figure 8I), indicating that the different HHT formulations did not induce neurotoxicity.

Collectively, these findings indicate a favorable in vivo safety profile of the HHT formulations.

https://doi.org/10.2147/IJN.S588865

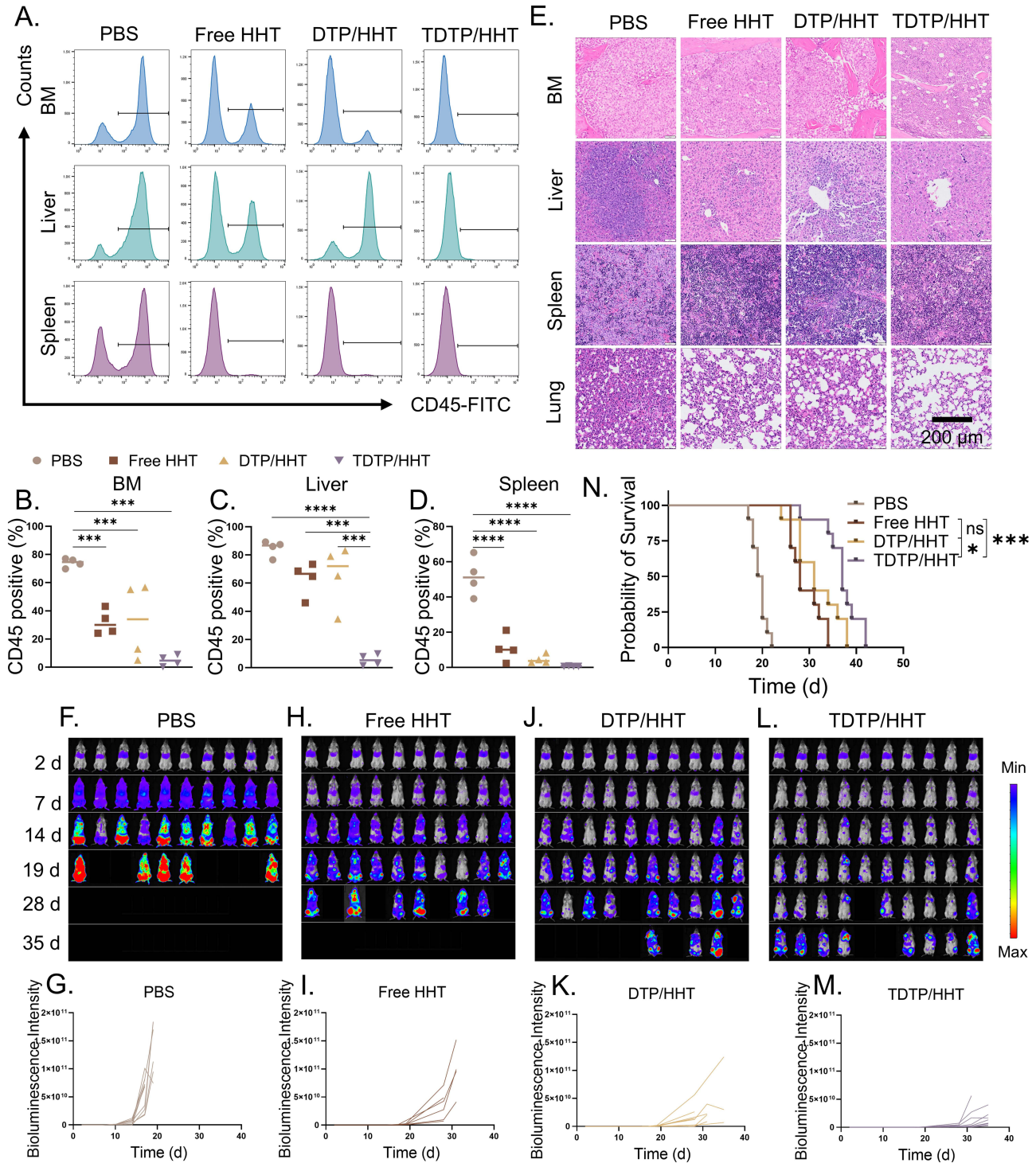

Figure 7 TDTP/HHT prolongs survival in AML xenograft mice. (**A**) Flow cytometry analysis of human $CD45^+$ cells in BM, liver, and spleen of AML xenograft mice. (**B**–**D**) Quantification of $CD45^+$ cell percentages in BM (**B**), liver (**C**) and spleen (**D**) (n=4). (**E**) Representative H&E-stained sections of leukemia-infiltrated organs. Scale bar=200 μm. (**F**–**M**) In vivo bioluminescence imaging of leukemia progression in mice treated with PBS (**F**), free HHT (**H**), DTP/HHT (**J**), and TDTP/HHT (**L**), with corresponding quantification of total bioluminescent signal intensity (**G, I, K, M**) at the indicated time points (n=10). (**N**) Kaplan-Meier survival curves of AML mice in different groups (n=10). *$p < 0.05$; ***$p < 0.001$; ****$p < 0.0001$; ns, not significant.

https://doi.org/10.2147/IJN.S588865

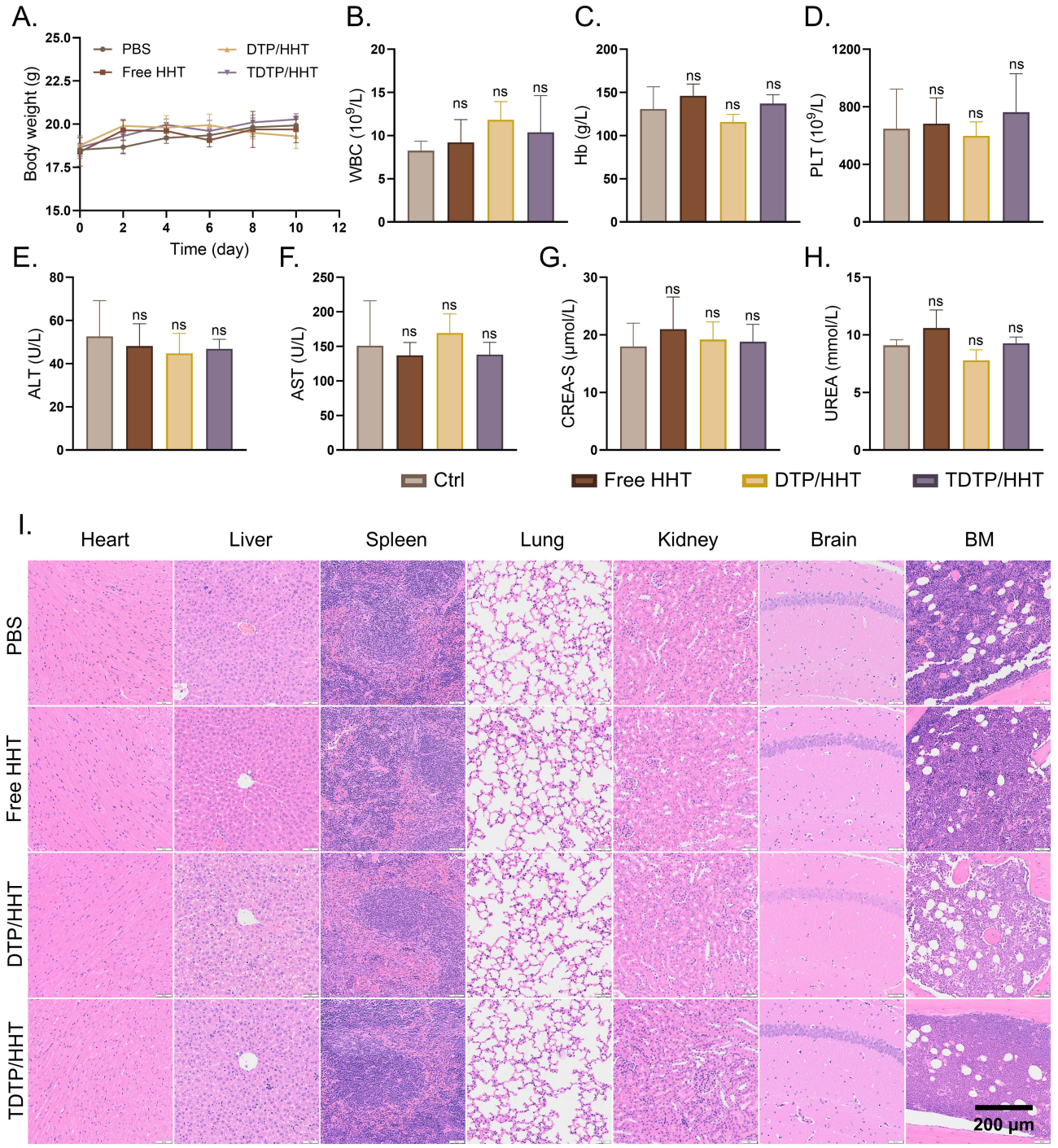

Figure 8 In vivo biocompatibility of different HHT formulations. (**A**) Body weight changes of mice during treatment (n=3). (**B**–**D**) Complete blood cell counts in different treatment groups (n=3), including white blood cells (**B**), hemoglobin (**C**), and platelets (**D**). (**E** and **F**) Liver function indicators (n=3), including ALT (**E**) and AST (**F**). (**G** and **H**) Kidney function indicators (n=3), including CREA-S (**G**) and UREA (**H**). (**I**) Representative H&E-stained sections of major organs. Scale bar=200 μm. ns, not significant.

Discussion

Current therapeutic strategies for FLT3-Mut AML rely on intensive induction chemotherapy combined with FLT3 inhibitors. However, their clinical efficacy is often limited by drug resistance, leading to relapse.[48–51] Additionally, the high cost of these targeted agents poses a significant barrier to widespread use in clinical practice. Therefore, HHT was therefore employed as an alternative due to its efficacy, affordability, and accessibility. Mechanistically, HHT binds to the

https://doi.org/10.2147/IJN.S588865

ribosomal A-site, thereby inhibiting protein synthesis and suppressing oncogenic proteins, ultimately promoting apoptosis in AML cells.[52,53] In this study, we demonstrated that FLT3-ITD AML cells are highly sensitive to HHT, with cytotoxicity comparable to the second-generation FLT3 inhibitor gilteritinib (Figure 2). In addition, TDTP/HHT formulation further enhanced efficacy through multitarget modulation in FLT3-ITD signaling. These findings suggest that HHT and its nanomedicine formulation may provide an alternative therapeutic option for AML patients with FLT3-ITD, particularly in the context of resistance to or limited accessibility of FLT3 inhibitors.

In healthy individuals, CD71, an early erythroid marker, is absent or expressed at very low levels on hematopoietic stem cells (HSC), becomes highly expressed in early erythroblasts due to increased iron demand, and markedly declines to near-negative levels upon maturation.[54,55] In AML, our data are consistent with earlier reports:[27] CD71 expression in AML cells is substantially higher than that in nucleated erythroid cells in the bone marrow, suggesting that CD71-targeted delivery systems can preferentially accumulate in AML cells. Although off-target effects on early erythroid cells may occur when disease burden decreases during remission, HSC and mature erythrocytes remain unaffected, indicating that such effects are controllable and reversible. Furthermore, our in vivo biocompatibility studies demonstrate that all HHT formulations did not induce hematological toxicity during treatment (Figure 8).

Current CD71-targeted NDDSs for AML often use monoclonal antibodies, ferritin or Tf,[29,56,57] all of which compete with endogenous Tf. Therefore, we incorporated the ^{D}T7 ligand, retro-inverso derivative of the CD71-specific binding peptide T7 identified through phage display screening.[35] The binding site of T7 on CD71 is distinct from that of Tf, thereby allowing endogenous Tf-driven endocytic trafficking to enhance the cellular internalization of T7-modified nanocarriers.[58,59] ^{D}T7 retains these binding characteristics while exhibiting enhanced CD71 affinity and improved serum stability.[36] Consequently, ^{D}T7-modified TDTP micelles demonstrated Tf-facilitated uptake without competitive inhibition (Figure 5). Further, the ROS-responsive design exploited the intrinsic oxidative stress within AML cells to achieve tumor-specific intracellular release of the HHT (Figures 3 and 4). Both in vitro and in vivo studies confirmed that TDTP/HHT exhibited significantly greater anti-leukemic activity than free HHT or non-targeted DTP/HHT micelles at equivalent doses (Figures 6 and 7). These results demonstrate that a dual-functional strategy guided by disease characteristics can effectively expand the therapeutic window of HHT.

Our design presents several features that may facilitate clinical translation: It is composed of simple constituents, features a reproducible preparation process, and avoids chemical modification of the parent drug. The HHT-only loaded pattern allows flexible combination with other chemotherapeutic agents since combination regimens remain the standard of care for AML. As HHT is commonly used in induction therapy, its incorporation into a nanocarrier platform may further enhance efficacy while reducing toxicity.

Nevertheless, several limitations should be acknowledged. First, our study remains at the preclinical stage and was primarily conducted in cell lines and cell-derived xenograft (CDX) models. CDX models do not fully recapitulate the complex tumor microenvironment of human AML, particularly the cellular composition and interactions within the bone marrow niche. In addition, prolonged in vitro culture may cause cell lines to lose key features and heterogeneity of primary tumors.[60] Therefore, future studies in patient-derived xenograft (PDX) models are warranted, as these models better preserve the clonal diversity and chemoresistant subpopulations of primary AML, which are critical for predicting clinical response.[61] Second, although primary AML samples were included in this study, the sample size remains limited and may not fully capture the biological heterogeneity of AML. Third, safety was evaluated by in vitro hemolysis and plasma stability, as well as short-term in vivo hematological analysis, histological examination and body weight monitoring, which collectively indicated a favorable biocompatibility profile. Nevertheless, these assessments were limited to short-term evaluation. As with many systemically administered nanomedicines, nanoparticles may undergo partial clearance by the reticuloendothelial system (RES), which can influence systemic circulation time and biodistribution.[62,63] Therefore, further pharmacokinetic and biodistribution studies are needed to evaluate RES uptake and systemic clearance. In addition, comprehensive long-term toxicity studies will be necessary, particularly to evaluate potential effects on the bone marrow hematopoietic microenvironment. Finally, ^{D}T7 is a short peptide ligand, and peptides generally exhibit lower immunogenicity compared with antibody-based systems.[64,65] Nevertheless, comprehensive immunological evaluation will be required in future studies to fully assess potential immune responses upon repeated administration. In addition, the current formulation delivers HHT alone. While this design provides flexibility for subsequent combination strategies, it precludes the convenience of co-delivering multiple agents within a single

nanoplatform. Future studies should explore the co-encapsulation of HHT with commonly used chemotherapeutics or novel targeted agents to construct multifunctional nanomedicines, thereby aiming to achieve an improved balance between efficacy and safety in clinical applications.

Conclusion

In summary, we have developed a dual-functional micellar delivery system that integrates CD71-targeting and ROS-responsiveness to enhance the therapeutic potential of HHT against FLT3-ITD AML, which is constructed based on FLT3-ITD features. The TDTP micelles demonstrated excellent CD71-mediated targeting without competing with endogenous Tf and Tf-facilitated cell uptake. Through multitarget inhibition of FLT3-ITD signaling, TDTP/HHT significantly improved anti-AML activity both in vitro and in vivo. While the enhanced efficacy was particularly evident in FLT3-ITD cells, TDTP/HHT also retained potency in FLT3-WT models with high CD71 expression, although higher doses was required to achieve comparable therapeutic effects. Together, these findings highlight the potential of this dual-functional nanocarrier to improve HHT delivery and efficacy across CD71-high AML, with especially enhanced responses observed in FLT3-ITD models. However, before clinical translation, comprehensive pharmacokinetic characterization and long-term systematic toxicity evaluation will be necessary to further assess the safety profile and therapeutic window of this nanomedicine platform.

Data Sharing Statement

The data used and analyzed during the current study are available from the corresponding author on reasonable request.

Ethics Approval and Informed Consent

This study was conducted in accordance with the Declaration of Helsinki and was approved by the Biomedical Ethics Committee of West China Hospital, Sichuan University (Approval No. 1182 (2024)). Written informed consent was obtained from all participants. All animal experiments were conducted in accordance with the institutional guidelines for the care and use of laboratory animals of West China Hospital, Sichuan University, and were approved by the Animal Ethics Committee of West China Hospital, Sichuan University (Approval No. 20241025003). The study was reported in accordance with the ARRIVE guidelines. At the experimental endpoint, mice were anesthetized with isoflurane and subsequently euthanized by cervical dislocation in accordance with the guidelines of the American Veterinary Medical Association.

Acknowledgments

We thank Dr. Fangfang Wang (Hematology Research Laboratory, West China Hospital, Sichuan University) for valuable technical support and experimental guidance. The authors further acknowledge Huaiqiang Sun, Jie Tu, and Feijing Su (Animal Imaging Core Facilities, West China Hospital, Sichuan University) for providing access to the imaging instruments used in this study.

Funding

This work was supported by the Science and Technology Department of Sichuan Province (grant number 2023YFS0307) and West China Hospital, Sichuan University (grant number 2023HXFH007).

Disclosure

The authors report no conflicts of interest in this work.

References

1. Kantarjian HM, DiNardo CD, Kadia TM, et al. Acute myeloid leukemia management and research in 2025. *CA Cancer J Clin*. 2025;75(1):46–67. doi:10.3322/caac.21873
2. Shallis RM, Daver N, Altman JK, et al. Standardising acute myeloid leukaemia classification systems: a perspective from a panel of international experts. *Lancet Haematol*. 2023;10(9):e767–e776. doi:10.1016/s2352-3026(23)00159-x
3. Anabtawi N, Nicolet D, Alotaibi N, et al. Prognostic, biological, and structural implications of FLT3-JMD point mutations in acute myeloid leukemia: an analysis of Alliance studies. *Leukemia*. 2025;39(3):623–631. doi:10.1038/s41375-024-02498-y

4. McInnes C. Overcoming Resistance to FLT3-ITD Therapeutics. *J Med Chem*. 2024;67(24):21749–21751. doi:10.1021/acs.jmedchem.4c02878
5. Lagunas-Rangel FA, Chávez-Valencia V. FLT3-ITD and its current role in acute myeloid leukaemia. *Med Oncol*. 2017;34(6):114. doi:10.1007/s12032-017-0970-x
6. Cortes J. Quizartinib: a potent and selective FLT3 inhibitor for the treatment of patients with FLT3-ITD-positive AML. *J Hematol Oncol*. 2024;17(1):111. doi:10.1186/s13045-024-01617-7
7. Kayser S, Schlenk RF, Londono MC, et al. Insertion of FLT3 internal tandem duplication in the tyrosine kinase domain-1 is associated with resistance to chemotherapy and inferior outcome. *Blood*. 2009;114(12):2386–2392. doi:10.1182/blood-2009-03-209999
8. Chen Y, Li S. Omacetaxine mepesuccinate in the treatment of intractable chronic myeloid leukemia. *Onco Targets Ther*. 2014;7:177–186. doi:10.2147/ott.S41786
9. Alvandi F, Kwitkowski VE, Ko CW, et al. U.S. Food and Drug Administration approval summary: omacetaxine mepesuccinate as treatment for chronic myeloid leukemia. *Oncologist*. 2014;19(1):94–99. doi:10.1634/theoncologist.2013-0077
10. Lü S, Wang J. Homoharringtonine and omacetaxine for myeloid hematological malignancies. *J Hematol Oncol*. 2014;7(1):2. doi:10.1186/1756-8722-7-2
11. Wang J, Lü S, Yang J, et al. A homoharringtonine-based induction regimen for the treatment of elderly patients with acute myeloid leukemia: a single center experience from China. *J Hematol Oncol*. 2009;2(1):32. doi:10.1186/1756-8722-2-32
12. Jin H, Zhang Y, Yu S, et al. Venetoclax Combined with Azacitidine and Homoharringtonine in Relapsed/Refractory AML: a Multicenter, Phase 2 Trial. *J Hematol Oncol*. 2023;16(1):42. doi:10.1186/s13045-023-01437-1
13. Yan D, Wei H, Lai X, et al. Co-delivery of homoharringtonine and doxorubicin boosts therapeutic efficacy of refractory acute myeloid leukemia. *J Control Release*. 2020;327:766–778. doi:10.1016/j.jconrel.2020.09.031
14. Kantarjian HM, Talpaz M, Santini V, Murgo A, Cheson B, O'Brien SM. Homoharringtonine: history, current research, and future direction. *Cancer*. 2001;92(6):1591–1605. doi:10.1002/1097-0142(20010915)92:6<1591::aid-cncr1485>3.0.co;2-u
15. Linet MS, Curtis RE, Schonfeld SJ, Vo JB, Morton LM, Dores GM. Survival of adult AML patients treated with chemotherapy in the U.S. population by age, race and ethnicity, sex, calendar-year period, and AML subgroup, 2001–2019. *EClinicalMedicine*. 2024;71:102549. doi:10.1016/j.eclinm.2024.102549
16. Daver N, Schlenk RF, Russell NH, Levis MJ. Targeting FLT3 mutations in AML: review of current knowledge and evidence. *Leukemia*. 2019;33(2):299–312. doi:10.1038/s41375-018-0357-9
17. Bacher U, Kern W, Schnittger S, Hiddemann W, Haferlach T, Schoch C. Population-based age-specific incidences of cytogenetic subgroups of acute myeloid leukemia. *Haematologica*. 2005;90(11):1502–1510.
18. Dong Y, Siegwart DJ, Anderson DG. Strategies, design, and chemistry in siRNA delivery systems. *Adv Drug Deliv Rev*. 2019;144:133–147. doi:10.1016/j.addr.2019.05.004
19. Zelikin AN, Ehrhardt C, Healy AM. Materials and methods for delivery of biological drugs. *Nat Chem*. 2016;8(11):997–1007. doi:10.1038/nchem.2629
20. Landesman-Milo D, Peer D. Transforming Nanomedicines From Lab Scale Production to Novel Clinical Modality. *Bioconjug Chem*. 2016;27(4):855–862. doi:10.1021/acs.bioconjchem.5b00607
21. Suk JS, Xu Q, Kim N, Hanes J, Ensign LM. PEGylation as a strategy for improving nanoparticle-based drug and gene delivery. *Adv Drug Deliv Rev*. 2016;99(Pt A):28–51. doi:10.1016/j.addr.2015.09.012
22. Belyaev IB, Griaznova OY, Yaremenko AV, Deyev SM, Zelepukin IV. Beyond the EPR effect: intravital microscopy analysis of nanoparticle drug delivery to tumors. *Adv Drug Deliv Rev*. 2025;219:115550. doi:10.1016/j.addr.2025.115550
23. Fang J, Nakamura H, Maeda H. The EPR effect: unique features of tumor blood vessels for drug delivery, factors involved, and limitations and augmentation of the effect. *Adv Drug Deliv Rev*. 2011;63(3):136–151. doi:10.1016/j.addr.2010.04.009
24. Daniels TR, Delgado T, Rodriguez JA, Helguera G, Penichet ML. The transferrin receptor part I: biology and targeting with cytotoxic antibodies for the treatment of cancer. *Clin Immunol*. 2006;121(2):144–158. doi:10.1016/j.clim.2006.06.010
25. Cheng Y, Zak O, Aisen P, Harrison SC, Walz T. Structure of the human transferrin receptor-transferrin complex. *Cell*. 2004;116(4):565–576. doi:10.1016/s0092-8674(04)00130-8
26. Wu X, Jiao Z, Zhang J, Li F, Li Y. Expression of TFRC helps to improve the antineoplastic effect of Ara-C on AML cells through a targeted delivery carrier. *J Nanobiotechnology*. 2023;21(1):126. doi:10.1186/s12951-023-01881-8
27. Wang C, Zhang W, He Y, et al. Ferritin-based targeted delivery of arsenic to diverse leukaemia types confers strong anti-leukaemia therapeutic effects. *Nat Nanotechnol*. 2021;16(12):1413–1423. doi:10.1038/s41565-021-00980-7
28. Wu W, Li Y, Liu Q, et al. Dual-Targeted Drug Delivery to Myeloid Leukemia Cells via Complement- and Transferrin-Based Protein Corona. *Nano Lett*. 2025;25(1):147–156. doi:10.1021/acs.nanolett.4c04429
29. Rajabinejad M, Valadan R, Tehrani M, et al. Effective delivery of anti-PD-L1 siRNA with human heavy chain ferritin (HFn) in acute myeloid leukemia cell lines. *Med Oncol*. 2024;41(6):149. doi:10.1007/s12032-024-02393-7
30. Hawkins GA, McCabe RP, Kim CH, et al. Delivery of radionuclides to pretargeted monoclonal antibodies using dihydrofolate reductase and methotrexate in an affinity system. *Cancer Res*. 1993;53(10 Suppl):2368–2373.
31. Kawabata H. Transferrin and transferrin receptors update. *Free Radic Biol Med*. 2019;133:46–54. doi:10.1016/j.freeradbiomed.2018.06.037
32. Salvati A, Pitek AS, Monopoli MP, et al. Transferrin-functionalized nanoparticles lose their targeting capabilities when a biomolecule Corona adsorbs on the surface. *Nat Nanotechnol*. 2013;8(2):137–143. doi:10.1038/nnano.2012.237
33. Wang X, Wang M, Lei R, Zhu SF, Zhao Y, Chen C. Chiral Surface of Nanoparticles Determines the Orientation of Adsorbed Transferrin and Its Interaction with Receptors. *ACS Nano*. 2017;11(5):4606–4616. doi:10.1021/acsnano.7b00200
34. Taylor EM, Otero DA, Banks WA, O'Brien JS. Retro-inverso prosaptide peptides retain bioactivity, are stable In vivo, and are blood-brain barrier permeable. *J Pharmacol Exp Ther*. 2000;295(1):190–194.
35. Lee JH, Engler JA, Collawn JF, Moore BA. Receptor mediated uptake of peptides that bind the human transferrin receptor. *Eur J Biochem*. 2001;268(7):2004–2012. doi:10.1046/j.1432-1327.2001.02073.x
36. Tang J, Wang Q, Yu Q, et al. A stabilized retro-inverso peptide ligand of transferrin receptor for enhanced liposome-based hepatocellular carcinoma-targeted drug delivery. *Acta Biomater*. 2019;83:379–389. doi:10.1016/j.actbio.2018.11.002
37. Sun Y, Liu X, Wang L, et al. High-performance SOD mimetic enzyme Au@Ce for arresting cell cycle and proliferation of acute myeloid leukemia. *Bioact Mater*. 2022;10:117–130. doi:10.1016/j.bioactmat.2021.08.012

38. Mondet J, Presti CL, Garrel C, et al. Adult patients with de novo acute myeloid leukemia show a functional deregulation of redox balance at diagnosis which is correlated with molecular subtypes and overall survival. *Haematologica*. 2019;104(9):e393–e397. doi:10.3324/haematol.2018.206821
39. Snezhkina AV, Kudryavtseva AV, Kardymon OL, et al. ROS Generation and Antioxidant Defense Systems in Normal and Malignant Cells. *Oxid Med Cell Longev*. 2019;2019:6175804. doi:10.1155/2019/6175804
40. Kannan S, Irwin ME, Herbrich SM, et al. Targeting the NRF2/HO-1 Antioxidant Pathway in FLT3-ITD-Positive AML Enhances Therapy Efficacy. *Antioxidants*. 2022;11(4):717. doi:10.3390/antiox11040717
41. Sallmyr A, Fan J, Datta K, et al. Internal tandem duplication of FLT3 (FLT3/ITD) induces increased ROS production, DNA damage, and misrepair: implications for poor prognosis in AML. *Blood*. 2008;111(6):3173–3182. doi:10.1182/blood-2007-05-092510
42. Sallmyr A, Fan J, Rassool FV. Genomic instability in myeloid malignancies: increased reactive oxygen species (ROS), DNA double strand breaks (DSBs) and error-prone repair. *Cancer Lett*. 2008;270(1):1–9. doi:10.1016/j.canlet.2008.03.036
43. Li X, Montague EC, Pollinzi A, Lofts A, Hoare T. Design of Smart Size-, Surface-, and Shape-Switching Nanoparticles to Improve Therapeutic Efficacy. *Small*. 2022;18(6):e2104632. doi:10.1002/smll.202104632
44. Salatin S, Maleki Dizaj S, Yari Khosroushahi A. Effect of the surface modification, size, and shape on cellular uptake of nanoparticles. *Cell Biol Int*. 2015;39(8):881–890. doi:10.1002/cbin.10459
45. Yao M, Yan W, Wang Y, et al. IHCH9033, a novel class I HDAC inhibitor, synergizes with FLT3 inhibitor and rescues quizartinib resistance in FLT3-ITD AML via enhancing DNA damage response. *Exp Hematol Oncol*. 2025;14(1):15. doi:10.1186/s40164-025-00605-y
46. Levis M. FLT3 mutations in acute myeloid leukemia: what is the best approach in 2013? *Hematology Am Soc Hematol Educ Program*. 2013;2013:220–226. doi:10.1182/asheducation-2013.1.220
47. McMahon CM, Ferng T, Canaani J, et al. Clonal Selection with RAS Pathway Activation Mediates Secondary Clinical Resistance to Selective FLT3 Inhibition in Acute Myeloid Leukemia. *Cancer Discov*. 2019;9(8):1050–1063. doi:10.1158/2159-8290.Cd-18-1453
48. Joshi SK, Nechiporuk T, Bottomly D, et al. The AML microenvironment catalyzes a stepwise evolution to gilteritinib resistance. *Cancer Cell*. 2021;39(7):999–1014.e8. doi:10.1016/j.ccell.2021.06.003
49. Kiyoi H, Kawashima N, Ishikawa Y. FLT3 mutations in acute myeloid leukemia: therapeutic paradigm beyond inhibitor development. *Cancer Sci*. 2020;111(2):312–322. doi:10.1111/cas.14274
50. Gebru MT, Wang HG. Therapeutic targeting of FLT3 and associated drug resistance in acute myeloid leukemia. *J Hematol Oncol*. 2020;13(1):155. doi:10.1186/s13045-020-00992-1
51. Antar AI, Otrock ZK, Jabbour E, Mohty M, Bazarbachi A. FLT3 inhibitors in acute myeloid leukemia: ten frequently asked questions. *Leukemia*. 2020;34(3):682–696. doi:10.1038/s41375-019-0694-3
52. Chen XJ, Zhang WN, Chen B, et al. Homoharringtonine deregulates MYC transcriptional expression by directly binding NF-κB repressing factor. *Proc Natl Acad Sci U S A*. 2019;116(6):2220–2225. doi:10.1073/pnas.1818539116
53. Mill CP, Fiskus W, DiNardo CD, et al. Effective therapy for AML with RUNX1 mutation by cotreatment with inhibitors of protein translation and BCL2. *Blood*. 2022;139(6):907–921. doi:10.1182/blood.2021013156
54. Dong HY, Wilkes S, Yang H. CD71 is selectively and ubiquitously expressed at high levels in erythroid precursors of all maturation stages: a comparative immunochemical study with glycophorin A and hemoglobin A. *Am J Surg Pathol*. 2011;35(5):723–732. doi:10.1097/PAS.0b013e31821247a8
55. Knaän-Shanzer S, van der Velde-van Dijke I, van de Watering MJ, et al. Phenotypic and functional reversal within the early human hematopoietic compartment. *Stem Cells*. 2008;26(12):3210–3217. doi:10.1634/stemcells.2007-0117
56. Suzuki S, Inoue K, Hongoh A, Hashimoto Y, Yamazoe Y. Modulation of doxorubicin resistance in a doxorubicin-resistant human leukaemia cell by an immunoliposome targeting transferring receptor. *Br J Cancer*. 1997;76(1):83–89. doi:10.1038/bjc.1997.340
57. Zhu Y, Zhang W, Chen J. Binary Nanodrug-Delivery System Designed for Leukemia Therapy: aptamer- and Transferrin-Codecorated Daunorubicin- and Luteolin-Coloaded Nanoparticles. *Drug Des Devel Ther*. 2023;17:1–13. doi:10.2147/dddt.S387246
58. Han L, Huang R, Li J, Liu S, Huang S, Jiang C. Plasmid pORF-hTRAIL and doxorubicin co-delivery targeting to tumor using peptide-conjugated polyamidoamine dendrimer. *Biomaterials*. 2011;32(4):1242–1252. doi:10.1016/j.biomaterials.2010.09.070
59. Oh S, Kim BJ, Singh NP, Lai H, Sasaki T. Synthesis and anti-cancer activity of covalent conjugates of artemisinin and a transferrin-receptor targeting peptide. *Cancer Lett*. 2009;274(1):33–39. doi:10.1016/j.canlet.2008.08.031
60. Bubnova X, Hope L, Wheadon H. Evaluation of current mouse in vivo models and advanced in vitro models for leukaemia research. *Blood Rev*. 2025;74:101318. doi:10.1016/j.blre.2025.101318
61. Kawashima N, Ishikawa Y, Kim JH, et al. Comparison of clonal architecture between primary and immunodeficient mouse-engrafted acute myeloid leukemia cells. *Nat Commun*. 2022;13(1):1624. doi:10.1038/s41467-022-29304-6
62. Wei Y, Quan L, Zhou C, Zhan Q. Factors relating to the biodistribution & clearance of nanoparticles & their effects on in vivo application. *Nanomedicine*. 2018;13(12):1495–1512. doi:10.2217/nnm-2018-0040
63. Alexis F, Pridgen E, Molnar LK, Farokhzad OC. Factors affecting the clearance and biodistribution of polymeric nanoparticles. *Mol Pharm*. 2008;5(4):505–515. doi:10.1021/mp800051m
64. Welling GW, Fries H. Choice of peptide and peptide length for the generation of antibodies reactive with the intact protein. *FEBS Lett*. 1985;182(1):81–84. doi:10.1016/0014-5793(85)81158-3
65. Liu M, Fang X, Yang Y, Wang C. Peptide-Enabled Targeted Delivery Systems for Therapeutic Applications. *Front Bioeng Biotechnol*. 2021;9:701504. doi:10.3389/fbioe.2021.701504